Supporting Information

Kinetics of Thermally Activated Triplet Fusion as a Function of Polymer Chain Packing in boosting the Efficiency of Organic Light Emitting Diodes

Amrita Dey[1], Naresh Chandrasekaran[1,2,3], Dwaipayan Chakraborty[4], Priya Johari[4*], Christopher R. McNeill[3], Akshay Rao[5], and Dinesh Kabra[1*]*

[1]*Department of Physics, Indian Institute of Technology Bombay, Powai, Mumbai (India) – 400076*

[2]*IITB-Monash Research Academy,* IIT Bombay*, Mumbai 400076, India*

[3]*Department of Materials Science and Engineering,* Monash University*, Wellington Road, Clayton, Victoria 3800, Australia*

[4]*Department of Physics, School of Natural Sciences, Shiv Nadar University, Greater Noida, Gautam Buddha Nagar, U.P. (India) – 201314*

[5]*Cavendish Laboratory, University of Cambridge, JJ Thomson Avenue, Cambridge, UK – CB3 0HE*

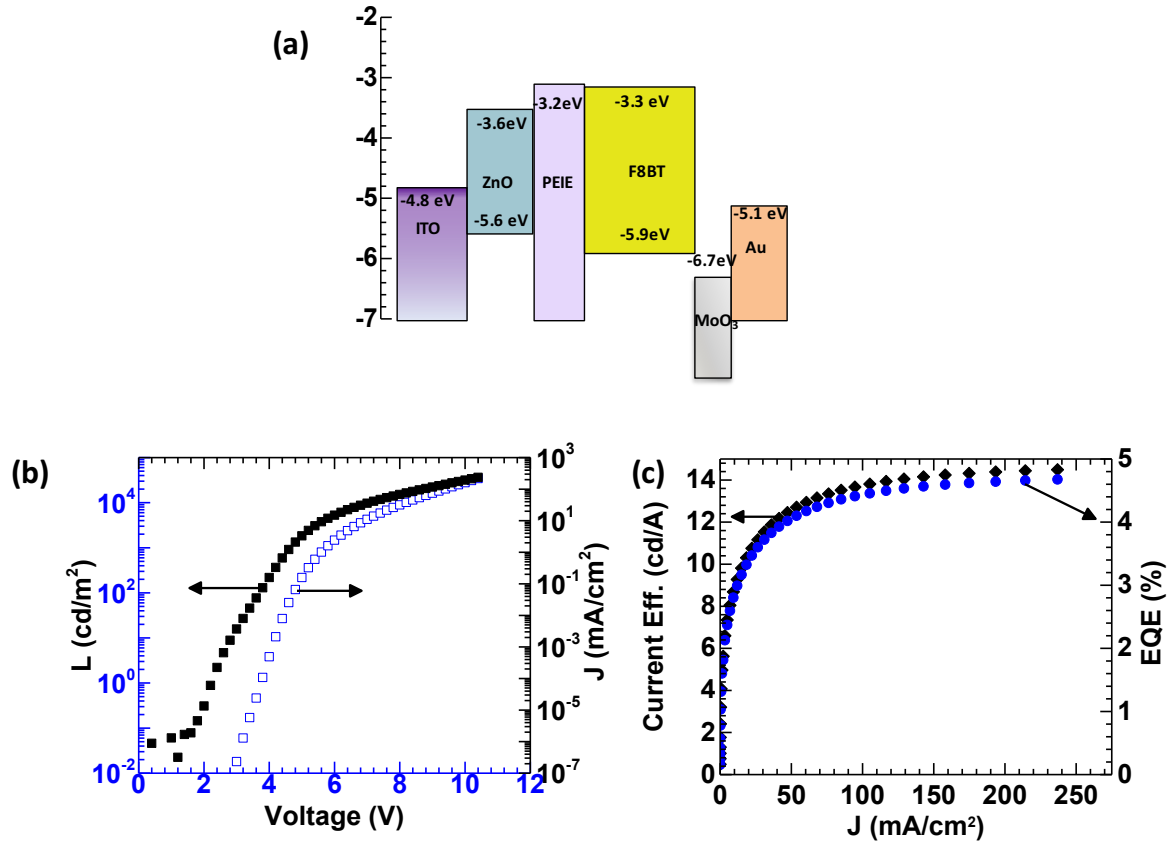

Figure S1. (a) Device structure for F8BT PLED and corresponding energy levels. **(b)** Current density (A/m^2)-Voltage-Luminance (cd/m^2) plot for F8BT PLED. **(c)** Current Efficiency (cd/A) and EQE (%) of the same device.

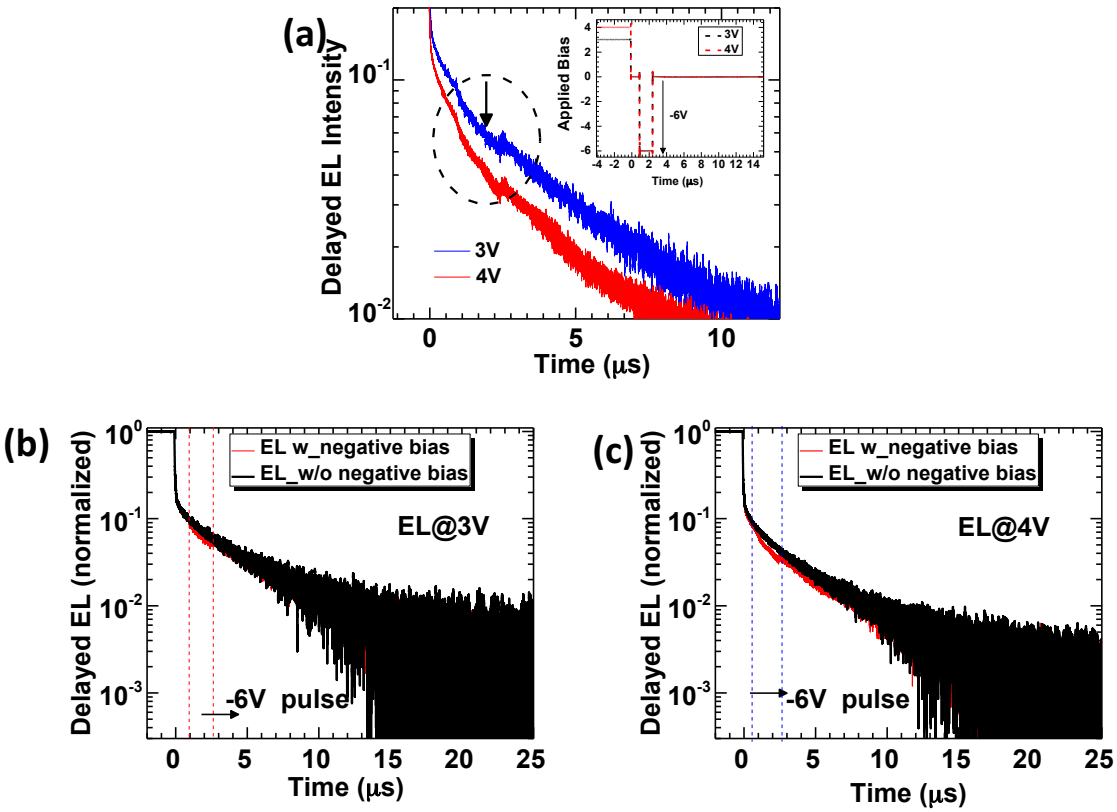

Figure S2. (a) Electrically stimulated DF emission from the F8BT PLEDs under a negative pulse of -6V height and ~2μs duration (applied after the end of positive bias voltage of height 3V and 4V). The negative pulse was adjusted to fall after 900ns from the ending of the main positive pulse as shown in the inset Figure. The DF gets quenched slightly during the negative pulse and remains almost unaffected after that as seen from the comparison of the DF decay dynamics in presence and absence of a negative pulse in the case **(b)** 3V positive voltage and **(c)** 4V positive voltage.

To verify the origin of DF emission under electrical excitation density a negative bias pulse of -6V has been applied to the PLED after ~900ns of the end of the positive electrical pulse (see in Figure S2b-S2d). It has been observed in the case of F8BT PLEDs the DF emission gets slightly quenched during the presence of negative bias pulse. However, the DF emission completely recovers once the negative bias gets switched off. The complete recovery of DF, clearly suggests that its origin in these devices is due to triplet excitons which are neutral to the applied negative electric field.[2,3]

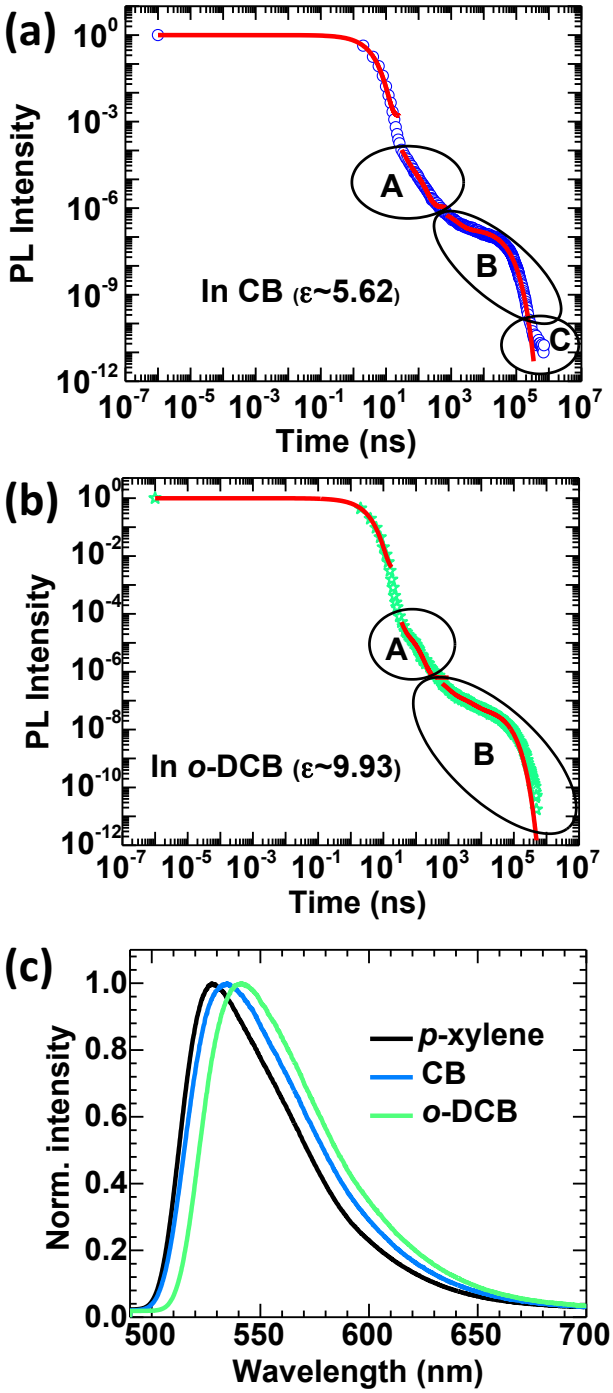

Figure S3. Solvent polarity dependent time-resolved photoluminescence decay of F8BT polymer in solution **(a)** Chlorobenzene (CB, ε~5.62) **(b)** o-di chlorobenzene (o-DCB, ε~9.93). With the increase in solvent polarity the DF lifetime increases as given in Table R1. **(c)** Steady-state PL intensity in F8BT solution of increased polarity. The PL spectra get red-shifted with an increase in solvent polarity.

We have performed time-resolved emission decay in F8BT as a function of increased solvent polarity (see in Figure S3). For this purpose, two other solvents, i.e., Chlorobenzene (CB: ε~5.65) and *o*-dichlorobenzene (*o* –DCB: ε~9.93) with higher polarity have been chosen. In case of all the solutions, F8BT's TRES decay reflects a transparent transition from PF to DF region at ~10's ns followed by a long-lived delayed emission component. The DF decay consists of three distinct luminescence decaying time regions for CB (see in Figure S3a) solution whereas for *o*-DCB (see in Figure S3b) there are two different regions. For each of the solution region, A has a faster exponential decay nature (which will be called DF1 now onwards) whereas region B has much slower exponential decay (which will be named DF2 from here onwards). Both DF1 and DF2 have bi-exponential decay ($I = I_0 + A_1 \exp(-t/\tau_1) + A_2 \exp(-t/\tau_2)$, I_0 and A_i are constants, with τ_i's are associated lifetimes). The fitted lifetimes for DF1 and DF2 are summarized in Table S1. Both DF1 and DF2 lifetime gets enhanced in the high polarity solvent where the PF lifetime also shows slight enhancement in the lifetime (Table S2). The third part of the delayed fluorescence region, i.e., region C (will be called DF3 here onwards) deviates from the exponential nature and follows a power law decay instead. A clear red-shifted emission is visible in the steady-state PL spectra (see Figure S3c) by enhancing the solvent polarity which signifies the charge transfer (CT) character of the F8BT polymer.[4]

Table S1: Solvent polarity dependent PF and DF lifetimes of the F8BT polymer.

Solution	**τ_{PF} (ns)**	**$\langle\tau_{DF1}\rangle$ (ns)**	**$\langle\tau_{DF2}\rangle$ (μs)**
p-xylene (ε~2.2)	2.23	12	20
CB (ε~5.62)	2.33	28	28
o-DCB(ε~9.93)	2.53	46	35

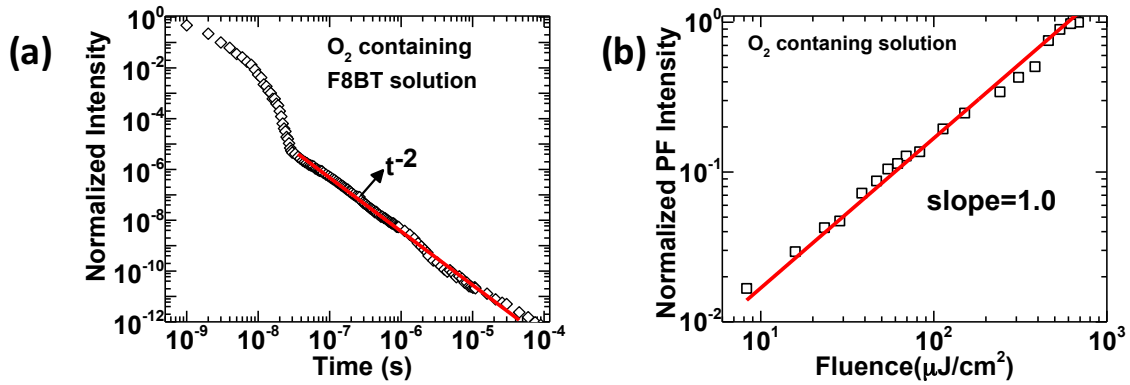

Figure S4 (a) Time-resolved PL decay of F8BT solution under O_2 atmosphere. The DF follows a t^{-2} power law decay. **(b)** Normalized PF vs. excitation fluence shows a unity sloe and thus rule out the possibility of SSA.

To verify the DF origin in F8BT solution due to triplet excitons we have measured the TRES in an aerated solvent (see in Figure S4a). The power law generated DF in case of the aerated solution (Figure S4a) may be considered as polaron pair[5,6] caused rather than triplet excitons made. Therefore, it is needed to be mentioned here; the polaron pair created DF decay shows a $\sim t^{-1.0}$ decay law[2,7] instead a $t^{-2.0}$ decay law which is most commonly treated as a signature of TTA.[2,8] Moreover, the primary cause of polaron pairs recombination generated delayed emission in solution media is singlet-singlet annihilation whose presence can be inferred from the excitation fluence dependent PF data.[7,9] But our excitation fluence dependent PF intensity in aerated solution shows a unity slope (see in Figure S4b), thus ruling out any essence of bimolecular singlet-singlet annihilation process.

Table S1.2: Thickness dependent photoluminescence lifetime values of F8BT films.

Thickness (nm)	Lifetime (ns)
110	1.75
310	1.86
560	2.17

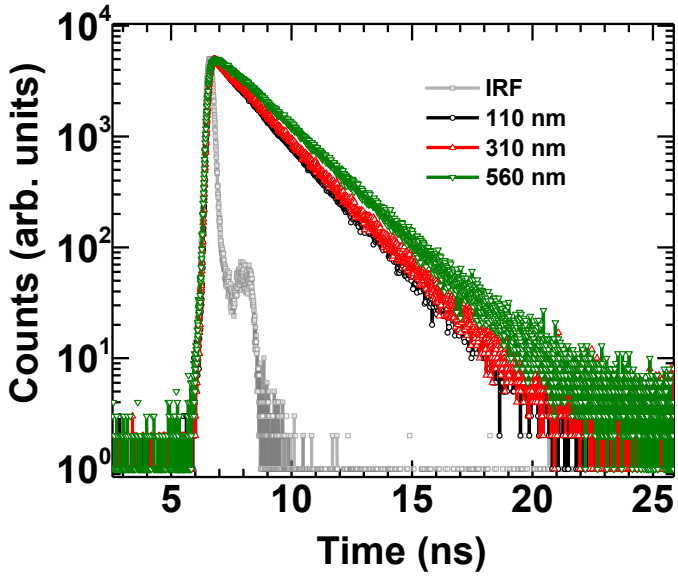

Figure S5. Thickness dependent lifetime measurement in F8BT films on quartz substrate using time correlated single photon counting (TCSPC).

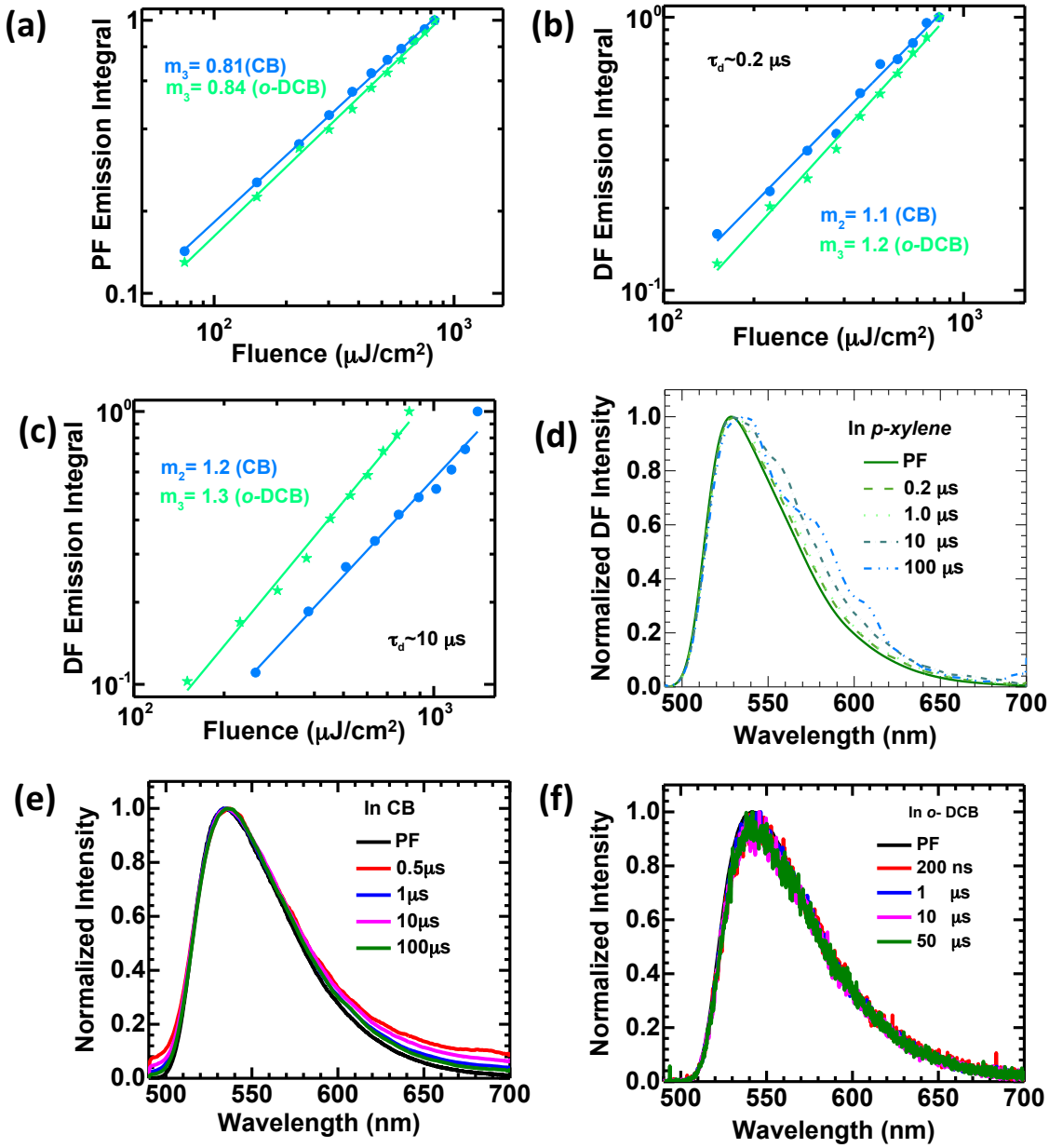

Figure S6. (a) PF intensity vs. excitation fluence as a function of solvent polarity. **(b)** Time-integrated DF1 intensity captured at 200ns time delay concerning excitation fluence**. (c)** Time-integrated DF2 intensity captured at 10μs time delay as a function of solvent polarity. PF and DF emission spectra at different time scale for **(d)** *p* –xylene **(e)** CB and **(f)** O-DCB as solvent media.

To know the origin of the DF from different regions in F8BT solution, the laser fluence dependent DF intensities have been recorded for DF1 and DF2 along with PF. The integrated PF intensity vs. laser fluence has been shown in Figure S6a for CB and *o*-DCB as solvent media. The PF vs. laser fluence dependency gives a slope ~0.84 for all the solutions of different polarities used in this study. In the solution media, DF1 and DF2 have a nearly linear

dependence on laser fluence as shown in Figure S6b and S6c for CB and *o*-DCB captured at the time delay ~200 ns and ~10 µs, respectively. The delayed fluorescence at different time delays in case of F8BT solution in CB and *o*-DCB can be seen Figure S6d and S6, respectively. The DF spectra in F8BT solution also matches with the PF Figure S6d to S6f.

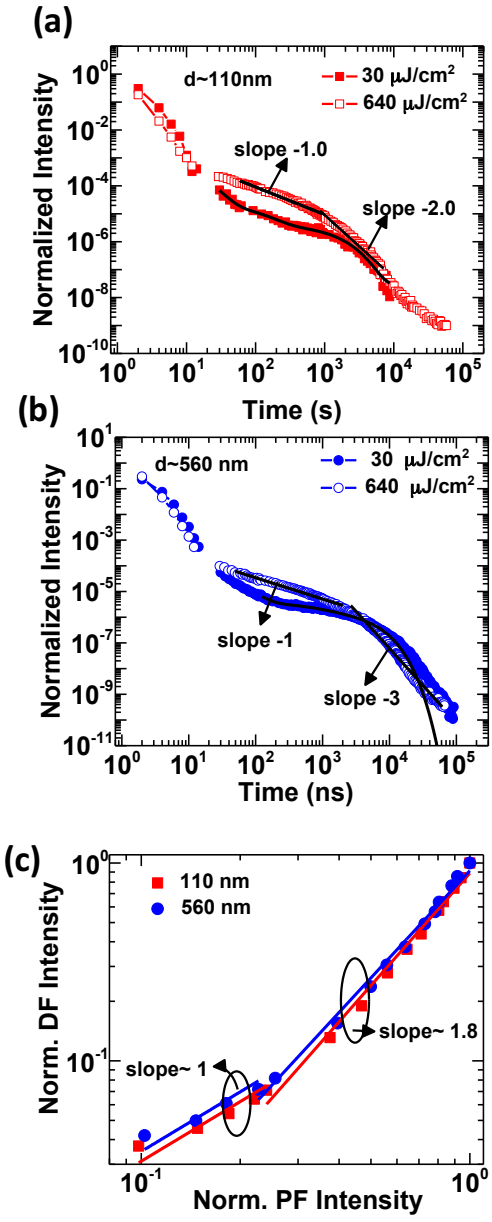

Figure S7. Gated time-resolved PL decay kinetics at low (~30 µJ/cm^2) and at high fluence (~640 µJ/cm^2) for F8BT films with **(a)** ~110 nm **(b)** ~560nm thicknesses. **(d)** Normalized DF emission integral vs normalized PF emission integral showing a linear DF intensity increment relative to PF intensity up to 100 µJ/cm^2 above which the DF intensity increases quadratically.

Figure S7a to **Figure S7b** show the excitation intensity dependent time-resolved PL decay of F8BT polymer films of different thicknesses, spin cast from varying polymer concentration in solution. Figure S7a shows the long-lived time-resolved PL decay kinetics for ~110nm thick F8BT film (recorded by intensified CCD using variable gate delay technique[1] _ENREF_30 under a dynamic vacuum of 10^{-5} mbar). The TRES decay consists of two parts; one is due to the prompt fluorescence (PF), and the other contribution is coming from the long-lived delayed fluorescence (DF) spanning up to hundreds of μs with PL intensity drops over several orders of magnitude. The complete kinetics have been captured at low (30 μJ/cm^2) and high fluence (640 μJ/cm^2) for all the polymer films. Figure S7b shows TRES decay for ~560nm F8BT films, respectively, as a function of excitation fluence. For all the film thicknesses, a definite turn over from PF to DF region is visible at ~10's ns. At low fluence, the DF intensity decays at a much slower pace with evident exponential features for all the three film thicknesses. At low fluence, the DF has a bi-exponential decay nature ($I = I_0 + A_1 \exp(-t/\tau_1) + A_2 \exp(-t/\tau_2)$) for thinnest film and follows a tri-exponential decay ($I = I_0 + A_1 \exp(-t/\tau_1) + A_2 \exp(-t/\tau_2) + A_3 \exp(-t/\tau_3)$) for ~560 nm thick films. The average DF lifetime $<\tau_{DF}>$ increases from 730ns for 110nm film to ~2.4 μs for the 560 nm film. It is observed that the non-exponential contribution increases in the DF decay with the increase in the film thickness, even at lower fluence. The DF decays much faster at high excitation fluence following power laws transiting from slope 1.2±0.1 at early times to nearly a slope ~3.0 at longer times, in case of all the film thicknesses studied here. **Figure S7c** shows an increase of normalized DF emission integral relative to normalized integrated PF emission intensity as a function of excitation fluence. For all the film thicknesses, the DF intensity follows a linear increase concerning PF intensity until 100 μJ/cm^2 beyond which DF follows a near quadratic rise relative to PF intensity.

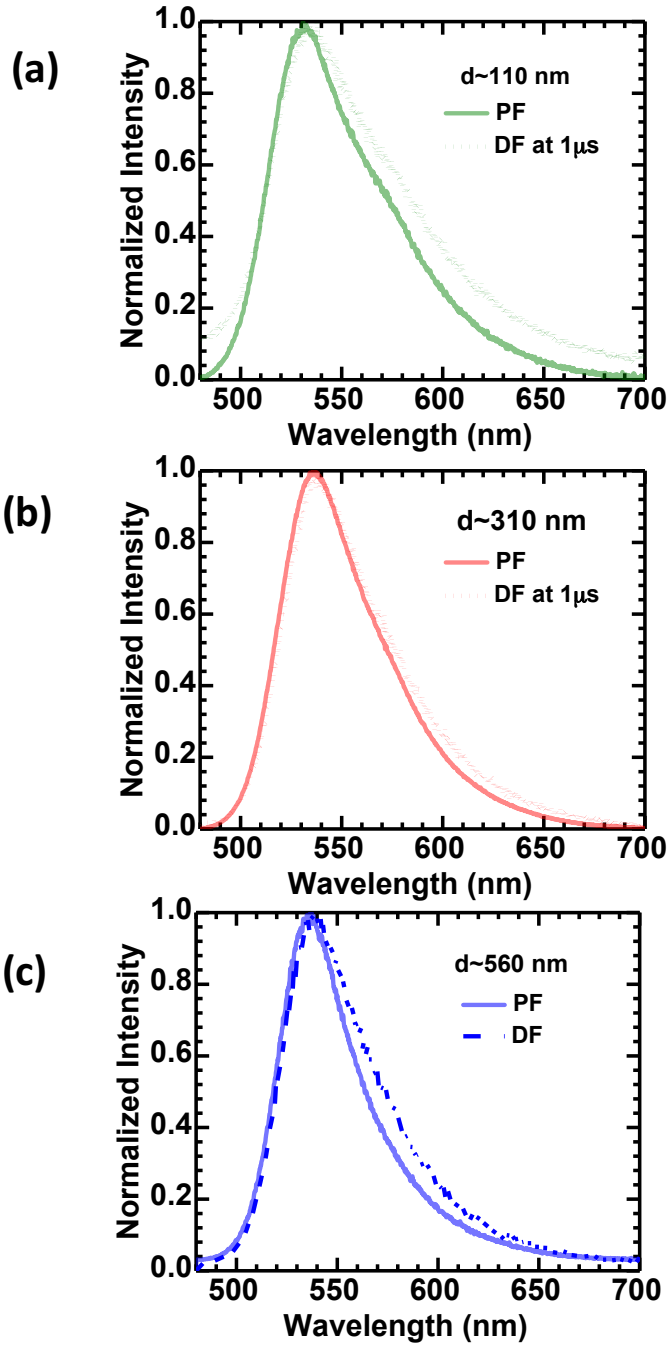

Figure S8. Prompt fluorescence and delayed fluorescence at one μs delay for **(a)** 110 nm and **(b)** 310 nm **(c)** 560 nm F8BT solid film, respectively. Both PF and DF emission get narrower with an increase in polymer film thickness due to more ordered polymer chain packing whereas the PL peak is red shifted due aggregation effect in thicker films.

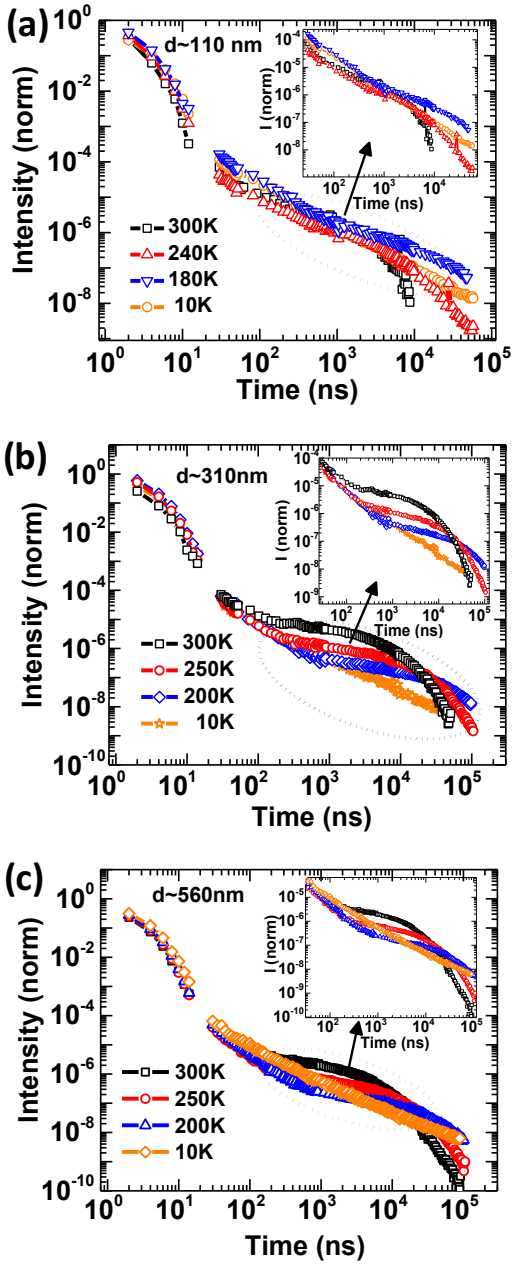

Figure S9. Temperature-dependent time-resolved PL decay for F8BT films of different thicknesses. Each decay curve has a fast and a slow component. **(a)** For thinnest film (~110 nm) the DF is almost remained unaffected relative to temperature, whereas **(b)** for intermediate thickness (~310 nm) and **(c)** thickest film (~560 nm) studied the DF decay dynamics changes from exponential to power-law decay at lower temperatures. The inset shows the magnified picture of the DF decays.

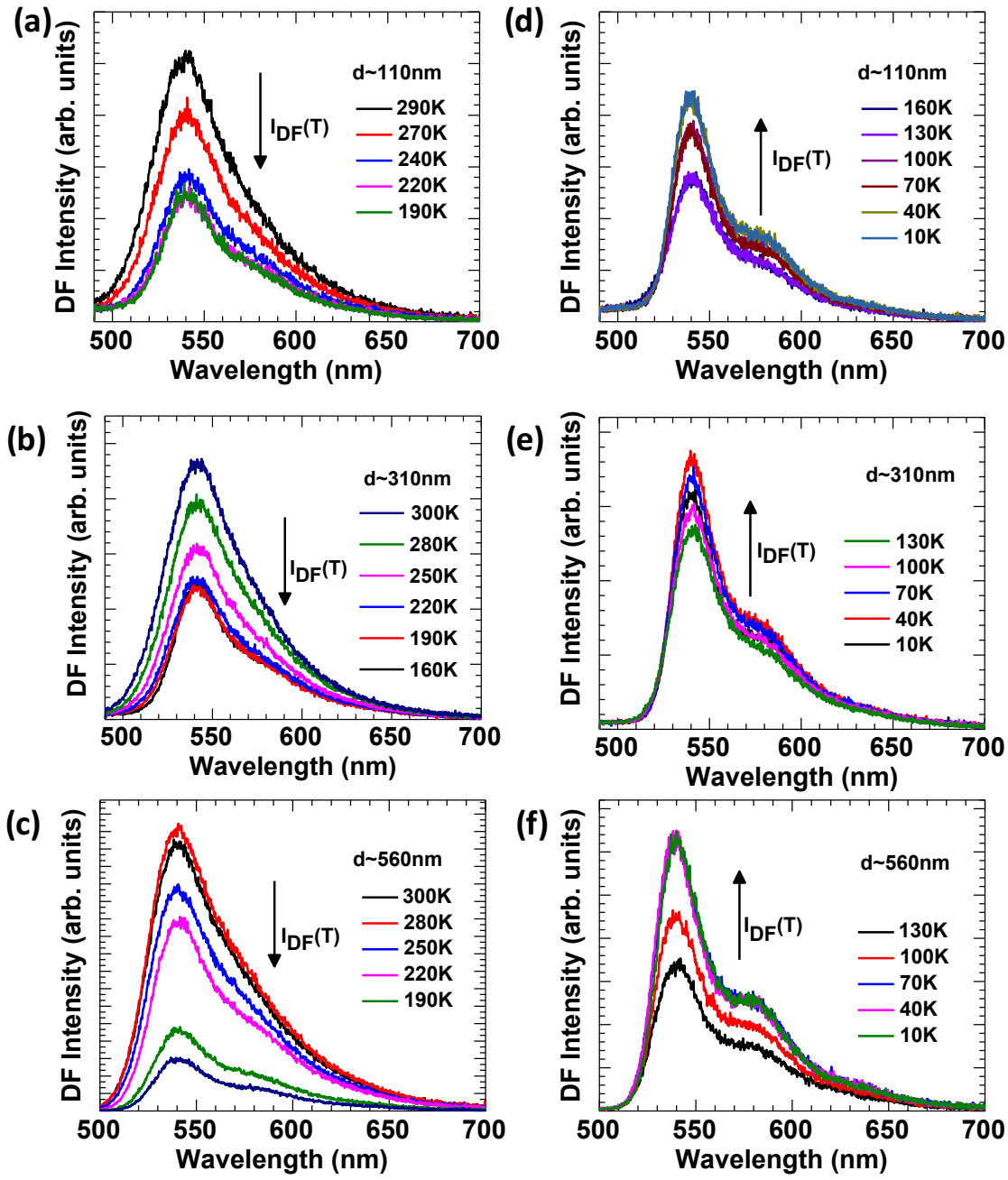

Figure S10. DF Intensity as a function of temperature for F8BT film of different thicknesses. **(a)** to **(c)** shows temperature activated region for DF intensity in case of ~110 nm ~310 nm and ~560 nm F8BT films, respectively, whereas Figures **(d)** to **(f)** temperature dependent tunneling regions for DF intensity for the similar thicknesses

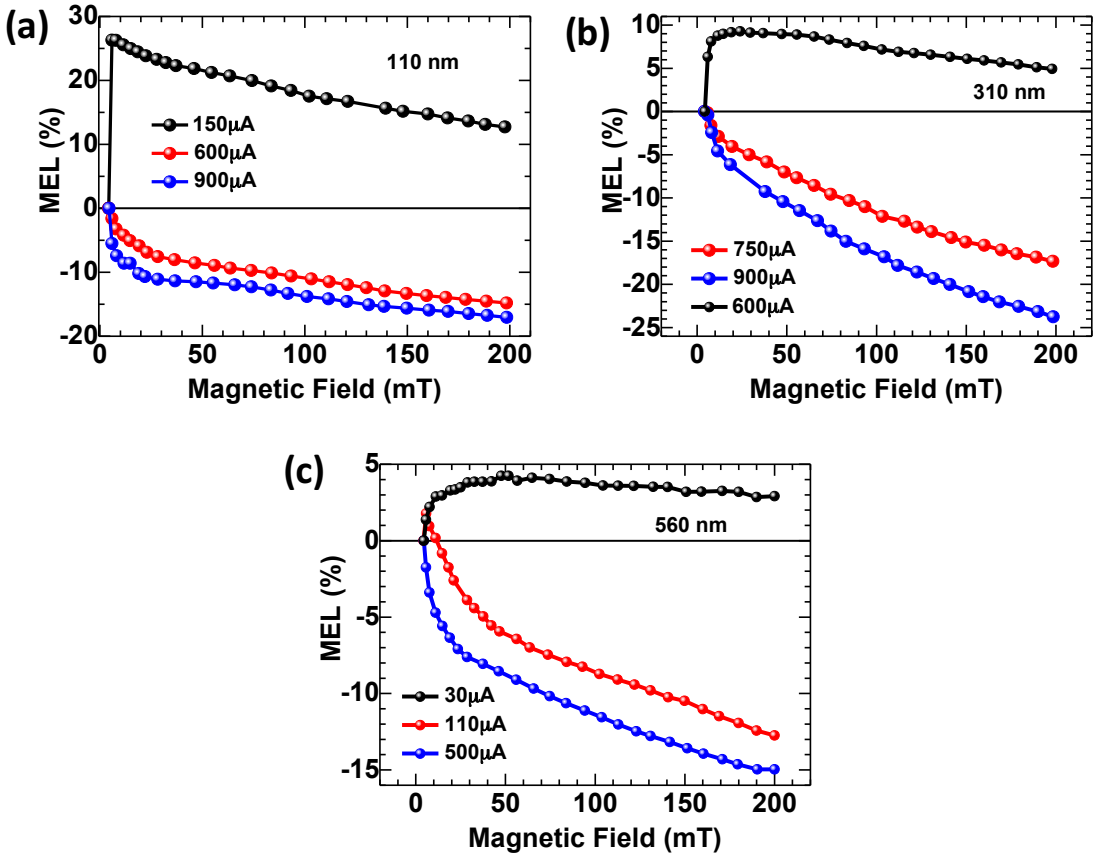

Figure S11. MEL response (EL(B)-EL(0)/EL(0)) under constant injection current mode of F8BT PLEDs (a) 110 nm (b)310 nm (c) 560 nm as emissive layer thickness. MEL response is positive at the low injection current level with an initial rise at the low applied magnetic field which starts to decrease at a field exceeding 50 mT for thick devices where for thinner devices the decrease happens at lower field. At high injection current, the MEL response becomes negative for all the emissive layer thicknesses. The MEL decay is faster for thinner devices as compared to thick devices.

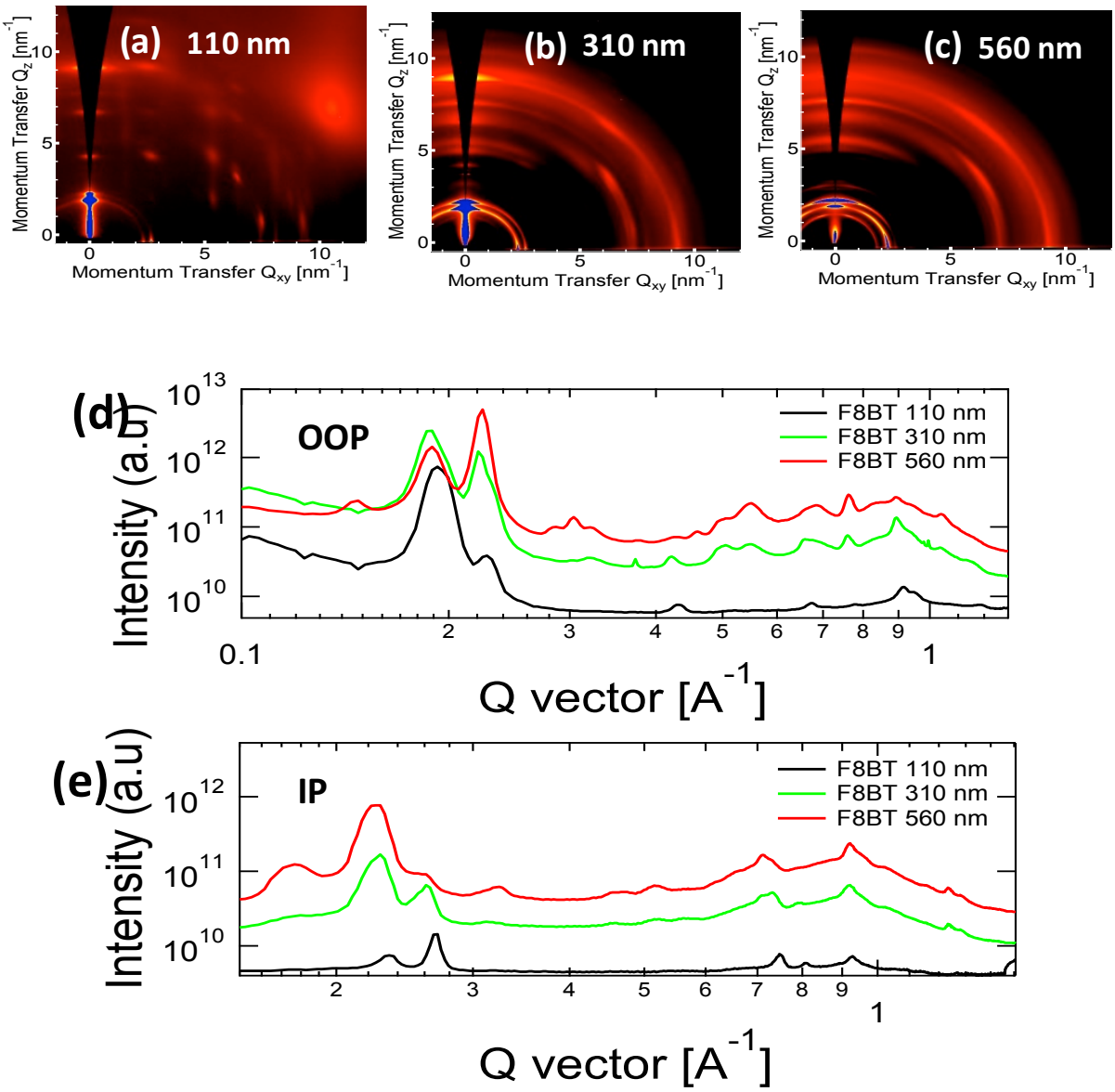

Figure S12. (a)- (c) 2D GIWAXS scattering images of F8BT thin films of different thickness over Si substrate. 1D scattering profile extracted from 2D GIWAXS image along **(d)** out-of-plane (OOP) direction and **(e)** in-plane(IP) for different thickness F8BT polymer films.

Grazing incident wide- angle X-ray scattering. GIWAXS measurements were performed at the SAXS/WAXS beamline at the Australian Synchrotron.[11] 15 keV photons were used with 2-dimensional scattering patterns recorded on a Dectris Pilatus 1M detector. Images shown in the manuscript were acquired at an incident angle close to the critical angle. Such images were chosen from a series of images taken with an incident X-ray angle varying from 0.02° to 0.15° in steps of 0.01° with the chosen image showing the highest scattering intensity. The X-ray exposure time was 1 s such that no film damage was identified. The sample-to-detector distance

was calibrated using a silver behenate sample. The results were analyzed by an altered version of the NIKA 2D[12] based in IgorPro.

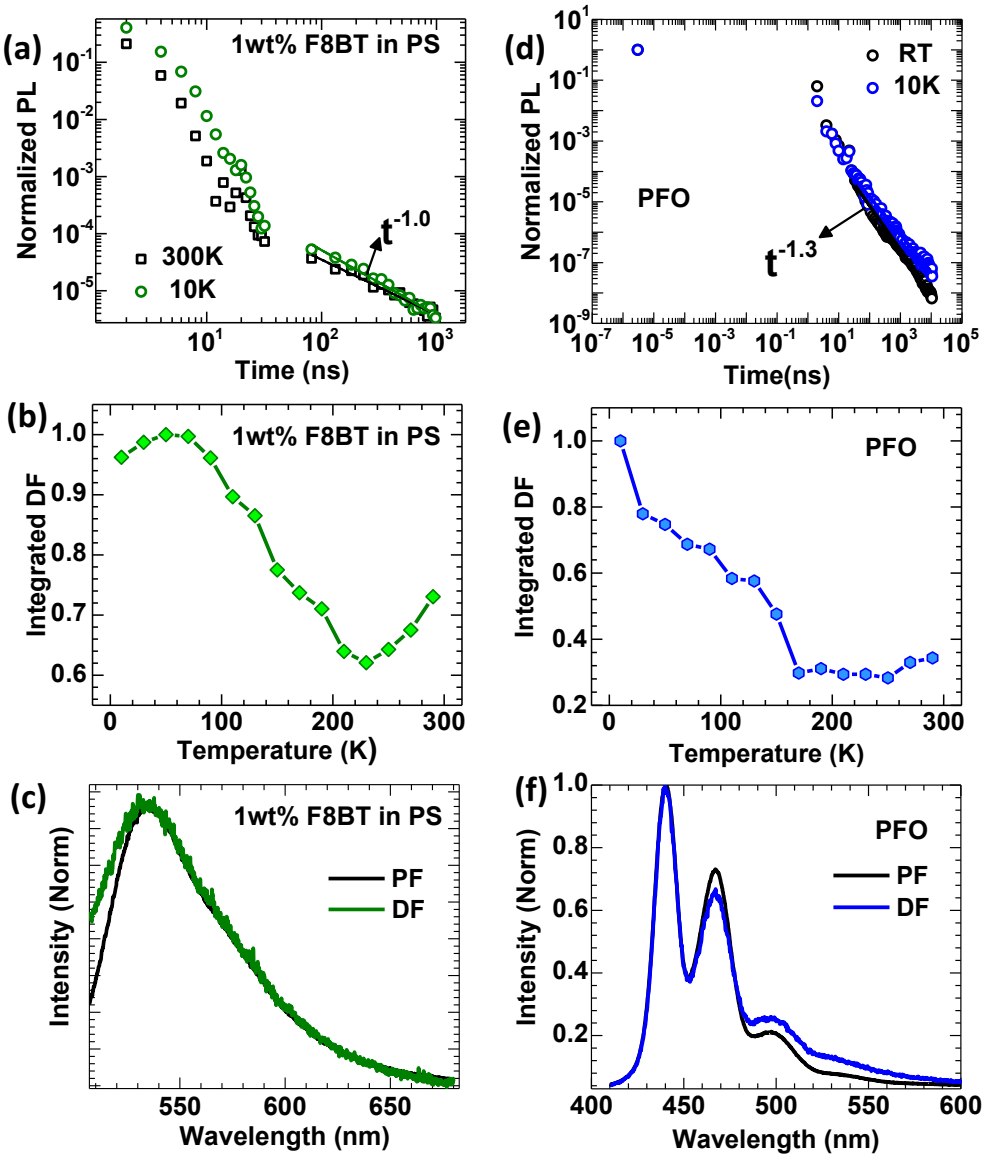

Figure S13. (a) Time-resolved emission kinetics in 1wt% F8BT dispersed in PS at room temperature (RT~300 K) and 10K. (b) DF intensity at a time delay of 200ns with an integration time of 1µs *vs.* temperature. (c) Prompt and delayed (200 ns) PL spectrum for F8BT dispersed in PS at room temperature. (d) Time-resolved emission kinetics in F8 film at room temperature (RT~300 K) and 10 K. (e) DF intensity at a time delay of 200ns with an integration time of 10µs *vs.* temperature for pristine F8 film. (f) Prompt and delayed (200 ns) PL spectrum for F8 film at room temperature.

Fluorene being a weak donor unit, the charge transfer character of F8BT is not so strong as also reflected by the solvent polarity dependent small stoke shift in the PL spectra (Figure S3c).

The dihedral angle between fluorene and benzothiadiazole unit is only ~15^0 as predicted from the PBC-DFT calculations.[13] This undermines the possibility of conventional TADF character (involving triplet to singlet reverse intersystem crossing) in this system. Besides that, the calculated energy gaps between S_1 and T_1 states are around 700 meV (as shown in Table S2) which are significantly larger than what is typically observed/reported in high-efficiency TADF OLED materials based on twisted D-A molecular architecture. It is to be noted that such a large energy gap value also seems quite consistent with the non-negligible spatial overlap between the HOMO and LUMO of F8BT, as depicted in Figure 1a in the manuscript. It is shown by Donley et al.[14] in the solid state the F8BT polymer chains form an "alternate structure" where adjacent neighboring polymer chains are shifted from each other in such a way that the 'F8' donor unit in one chain faces the acceptor 'BT' unit of the neighboring chain. Also, the interchain energy transfer is much stronger than intrachain energy transfer in case of F8BT. TADF being an intramolecular process should be reflected in the dispersive film in an inert matrix. To further clarify the DF origin in F8BT, we have measured temperature dependent TRPL in 1wt% F8BT dispersed in inert PS (polystyrene) matrix and only F8 (PFO) polymeric system.

Dispersed F8BT film in an inert matrix (**Figure S13a**) doesn't show any temperature dependent DF decay. Both at room and low temperature the DF decay follows a power law ~$t^{-1.3}$. The corresponding DF intensity is less dependent on temperature from 300 K to 250 K range as seen in **Figure S13b.** After that, DF intensity increases rapidly and achieves almost a temperature independent value below 70 K. The similar behavior has been observed in case of only donor polyfluorene (F8) unit (**Figure S13c).** Time-resolved PL decay in case of Polyfluorene follows power law decay (~$t^{-1.3}$) both at room temperature and low temperature showing the minimal effect on decay pattern. The DF intensity (**Figure S13d)** remains almost independent of temperature till 150 K below which it increases rapidly up to 70 K and then slowly increases with lowering the temperature. The contrasting behavior of temperature

dependent PL decay of F8BT from dispersed F8BT in inert matrix suggests that thermally assisted triplet energy transfer in F8BT is a strongly interchain process where solid chain packing controls triplet energy transport and thus the efficiency of DF.

S.2.1. Computational Details:

The ground state geometry of the F8BT molecule and the relaxed structure of F8BT molecules with different dihedral angle (Φ; manually fixed) between the donor and the acceptor moieties was obtained using density functional theory (DFT) based method, as implemented in Gaussian 09 software package,[15] using B3LYP[16,17] level of theory with 6-311+G(d, p) basis set.[18,19] The harmonic oscillator frequency calculations were also performed to confirm that the optimized structure is at the global minima of the potential energy surface. The optimized geometry of each molecule was obtained by considering atomic forces to be less than 0.0005 atomic unit (a.u.), while the convergence criteria for energy and density was set to 10^{-6} and 10^{-8} a.u., respectively.

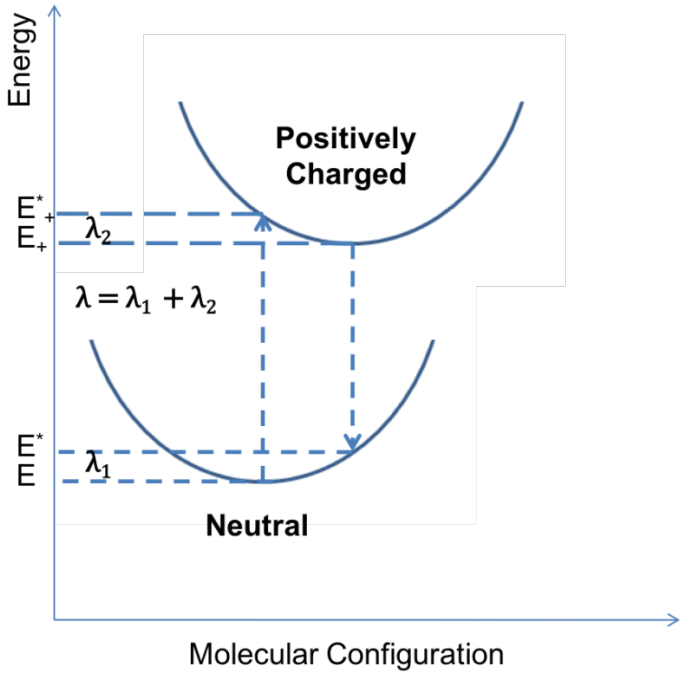

Figure S14: Schematic representation of the potential energy surfaces of neutral and charged molecules. The reorganization energy is calculated as: $\lambda = \lambda_1 + \lambda_2$, where λ_1/λ_2 represents the energy difference between neutral/charged configurations of neutral and charged molecules. E and E_+ denote the energy of the relaxed neutral and charged molecules, respectively, while E^*

gives the energy of the neutral configuration of optimized positively charged geometry, and E^*_+ is the energy of the charged configuration of optimized neutral geometry.

The reorganization energy (λ) is mainly comprised of two parts: the internal part, which is associated with the fast changes in molecular configurations due to charge transfer and the external part, that describes the changes due to the polarization of the surrounding solvent molecules. Here, we neglect the contribution of the external part while calculating λ because a spin triplet excited state is overall charge neutral, and thus, it is less sensitive to the polarization effects of the environment.[20] Figure S14 depicts a schematic diagram for calculation of λ from the adiabatic potential surfaces of neutral and charged molecular configurations, within the framework of Marcus-Hush theory.[21]

As shown in the Figure S1, the reorganization energy is calculated using the expression:

$$\lambda = \lambda_1 + \lambda_2 = (E^* - E) + (E^*_+ - E_+).$$

Here, E and E_+ represent the energy of the relaxed neutral and charged molecules, respectively, while E^* gives the energy of the neutral configuration of optimized positively charged geometry and E^*_+ is the energy of the charged configuration of optimized neutral geometry.

To estimate the contribution of the TTA process in explaining the high efficiency of F8BT polymer based PLEDs, the singlet (E_{S1}) and triplet (E_{T1}) excitation energies corresponding to the ground state to lowest singlet and triplet excited state transitions, respectively, were calculated using time-dependent density functional theory (TDDFT)[22,23] as implemented in Gaussian09 software suite. We computed lowest 25 singlet-singlet and 25 single-triplet transitions for all molecules by adopting the B3LYP*xc*-functional, along with the same basis set used for DFT calculations. It is well reported that B3LYP *xc*-functional gives a good description of singlet, triplet energy states[23] and thus, singlet-triplet energy splitting (ΔE_{ST}) and the ratio, E_{T1}/E_{S1}.

S.2.2.Optimized geometry of F8BT molecule:

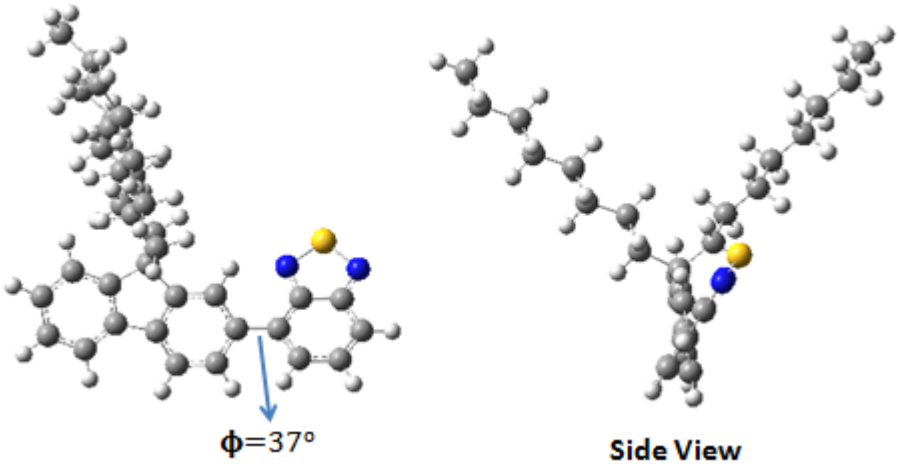

Figure S15: Front (left) and the side (right) view of the optimized structure of F8BT. Here, **Φ** represents the dihedral angle between the donor (F8) and the acceptor (BT) moieties.

S.2.3. Lowest single-triplet excited state transition energy:

Table S2. Variation in the lowest singlet (E_{S1}) and triplet (E_{T1}) exciton energy, ΔE_{ST} (=E_{S1}-E_{T1}), and E_{T1}/E_{S1} with respect to the dihedral angle (**Φ**) between the donor and the acceptor moieties of F8BT.

	Φ=50°	**Φ=37°**	**Φ=30°**	**Φ=25°**	**Φ=20°**	**Φ=15°**
E_{S1}(eV)	2.80	2.76	2.74	2.72	2.70	2.68
E_{T1}(eV)	2.05	1.98	1.94	1.91	1.89	1.86
ΔE_{ST}(eV)	0.75	0.78	0.80	0.81	0.81	0.82
E_{T1}/E_{S1}	0.732	0.717	0.708	0.702	0.700	0.694

References:

1. Rothe, C. & Monkman, A. Regarding the origin of the delayed fluorescence of conjugated polymers. *The Journal of chemical physics* 123, 244904 (2005).
2. Hertel, D., Bässler, H., Guentner, R. & Scherf, U. Triplet-triplet annihilation in a poly(fluorene)-derivative. *The Journal of Chemical Physics* **115**, 10007-10013, (2001).doi:10.1063/1.1415446
3. King, S. M. *et al.* The contribution of triplet-triplet annihilation to the lifetime and efficiency of fluorescent polymer organic light emitting diodes. *Journal of Applied Physics* **109**, 074502, (2011).doi:http://dx.doi.org/10.1063/1.3561430
4. Petrozza, A., Laquai, F., Howard, I. A., Kim, J.-S. & Friend, R. H. Dielectric switching of the nature of excited singlet state in a donor-acceptor-type polyfluorene copolymer. *Physical Review B* **81**, 205421 (2010).

5. Noolandi, J. & Hong, K. M. Theory of photogeneration and fluorescence quenching. *The Journal of Chemical Physics* 70, 3230-3236, (1979).doi:10.1063/1.437912
6. Reufer, M. et al. Spin-conserving carrier recombination in conjugated polymers. Nat Mater2005 Apr. 4,3406
7. Gélinas, S. et al. Recombination Dynamics of Charge Pairs in a Push-Pull Polyfluorene-Derivative. *The Journal of Physical Chemistry B* 117, 4649-4653 (2012).
8. Jankus, V., Chiang, C. J., Dias, F. & Monkman, A. P. Deep Blue Exciplex Organic Light- Emitting Diodes with Enhanced Efficiency; P- type or E- type Triplet Conversion to Singlet Excitons? *Advanced Materials* 25, 1455-1459 (2013).
9. Stevens, M. A., Silva, C., Russell, D. M. & Friend, R. H. Exciton dissociation mechanisms in the polymeric semiconductors poly(9,9-dioctylfluorene) and poly(9,9-dioctylfluorene-co-benzothiadiazole). *Physical Review B* 63, 165213 (2001).
10. Ogiwara, T., Wakikawa, Y. & Ikoma, T. Mechanism of intersystem crossing of thermally activated delayed fluorescence molecules. *The Journal of Physical Chemistry A* **119**, 3415-3418 (2015).
11. Kirby, N. M., Mudie, S. T., Hawley, A. M., Cookson, D. J., Mertens, H. D. T., Cowieson, N., and Samardzic-Boban, V, A low background intensity focusing small angle X-ray scattering undulator beamline, .J. Appl. Cryst. 2013, 46, 1670
12. Ilavsky, I., Nika: software for two dimensional data reduction, J. Appl. Cryst. 2012, 45, 324.
13. Eslamibidgoli, M. J. & Lagowski, J. B. The Effect of Side-Chain Length on the Solid-State Structure and Optoelectronic Properties of Fluorene-alt-Benzothiadiazole Based Conjugated Polymers A DFT Study. *The Journal of Physical Chemistry A* **116**, 10597-10606 (2012).
14. Donley, C. L. *et al.* Effects of Packing Structure on the Optoelectronic and Charge Transport Properties in Poly(9,9-di-n-octylfluorene-alt-benzothiadiazole). *Journal of the American Chemical Society* **127**, 12890-12899, (2005). doi:10.1021/ja051891j
15. Frisch, M. J., Trucks, G. W., Schlegel, H. B., Scuseria, G. E., Robb, M. A., Cheeseman, J. R., Scalmani, G., Barone, V., Mennucci, B., Petersson, G. A. *et al.* Gaussian 09, Gaussian, Inc.: Wallingford, CT, (2009).
16. Becke, A. D. Density-functional thermochemistry. iii. the role of exact exchange *J. Chem. Phys.* **98**, 5648−5652 (1993).
17. Lee, C., Yang, W. & Parr, R. G. Development of the Colle-Salvetti correlation-energy formula into a functional of the electron density *Phys. Rev. B: Condens. Matter Mater. Phys.* **37**, 785−789 (1988).
18. McLean, A. D. & Chandler, G. S. Contracted Gaussian Basis Sets for Molecular Calculations. I. Second Row Atoms, Z = 11−18. *J. Chem. Phys.***72,** 5639−5648 (1980).
19. Wachters, A. J. H. Gaussian Basis Set for Molecular Wavefunctions Containing Third-Row Atoms. *J. Chem. Phys.* **52**, 1033−1036 (1970)
20. Fishchuk, I. I. *et al.* Triplet energy transfer in conjugated polymers. II. A polaron theory description addressing the influence of disorder. *Physical Review B* **78**, 045211 (2008).
21. R., Marcus. *Chemical* and Electrochemical Electron-Transfer Theory. Annual Review of Physical *Chemistry. Annu. Rev. Phys. Chem.* ***15,*** *155-196 (1964)*
22. Runge, E. & Gross, E.K.U. Density-functional theory of time-dependent systems. *Phys. Rev. Lett.* **52,** 997-1000 (1984)
23. Marques, M.A.L, Ullrich, C.A., Nogueira, F., Rubio, A., Burke, K. & Gross, E.K.U. Time-dependent density functional theory, in *Lecture Notes in Physics* vol.-706, Springer-Verlag, Berlin, Heidelberg (2006)